I-B ANALYTICAL MODELING OF FIRE GROWTH ON FIRE-RESISTIVE WOOD-BASED MATERIALS WITH CHANGING CONDITIONS

Mark A. Dietenberger
USDA, Forest Service
Forest Products Laboratory
Madison, WI

ABSTRACT

Our analytical model of fire growth for the ASTM E 84 tunnel, which simultaneously predicts heat release rate, flame-over area, and pyrolysis area as functions of time for constant conditions, was documented in the 2001 BCC Symposium for different treated wood materials. The model was extended to predict ignition and fire growth on exterior fire-resistive structures and ornamental vegetation for an efficient assessment of fire hazard in the wildland–urban interface. The improved model accommodates the following changing conditions: (1) transient variation of imposed heat fluxes in pyrolysis and flame-over regions, (2) non-linearity in flame-over lengths, (3) transient changes in environmental conditions, and (4) transition in flame spreading from thermally thick to thin behavior. Re-validation of the updated model with an ISO 9705 room-burn series that contained upward fire spread data is in process and will be presented at the proceedings. Cone calorimeter data for fire-resistive materials such as redwood, fire-resistant-treated plywood, and single-layer stucco-coated oriented strandboard were used in the validation work. Burning characteristics of Class B brand used in the ASTM E 108 test were also determined in a specialized cone calorimeter test to help guide model development.

INTRODUCTION

With increasing fire hazards from wildfires, particularly in the southwestern United States, homebuilders in the wildland–urban interface (WUI) will come under increasing regulatory pressure to adopt exterior fire-resistive structures and manage landscape vegetation. However, the effective strategy for wildfire mitigation is not always clear, even to a fire protection expert. Indeed, homeowners and builders could benefit greatly from a calculation tool for evaluating wildfire hazards to their structures. Fire threats in the WUI basically come in two forms: (1) long-duration exposure from firebrand spotting and (2) short-duration exposure from heat flux or flame impingement of the wildfire nearing the structure.

The fire hazard threat of high heat flux or flame impingement from short-duration wildfire exposure is primarily mitigated with vegetative management in the defense zones around the combustible structure. The kind of vegetative management needed to prevent structural ignition depends on fire resistance of the construction, moisture condition of landscape vegetation, and positions and types of ornamental vegetations relative to the combustible structure. To establish the non-threatening distances of rapidly burning ornamental vegetations from a given structure, which may or may not be fire resistant, one should ideally use a fire hazard calculation tool, such as that partially developed in this paper. The insidious threat from long-duration exposure to firebrands, particularly those blown from a large distant wildfire, is the main driving force for requiring fire-resistant structures in the WUI. Obviously, homeowners need to place wire screens over chimneys and vents and around decks and some windows to prevent ember penetration into the highly combustible interiors of buildings (Manzello and others, 2006). However, how much exterior fire resistance is needed is not clear. The homeowner could decide that the wood deck is expendable as long as the fire (possibly originating from firebrands in a crevice on the cedar deck, Manzello and others, 2006) does not spread into the fire-resistant home. The patio door and windows should also be made resistant to the worst-case firebrand, which is likely the Class A or B simulated firebrand in the ASTM E 108 test. The Class A firebrand can also be thought of as multiple firebrands collecting in a corner wall, where the upward flame spread on combustible siding is likely. The use of an exterior FRT wood siding or similarly fire-resistive material will instead prevent such flame spread, thereby limiting damage or ignition to the region of direct exposure from the firebrands. The main point of this discussion is that even with effective vegetative management, reasonable and economical design using exterior fire-resistant materials should be considered in preparing for the threat of firebrands.

Computing speeds have reached the point of enhancing real-time calculation of damage, ignition, and fire growth on combustible objects. Because computational fluid dynamics (CFD) codes such as the Fire Dynamics Simulator (FDS) are far from reaching such a point, we present here certain analytical solutions of the dynamic processes of surface heating to ignition and then finally to fire growth. The key numerical procedure is using stepping boundary conditions to discretize the analytical time integration, which then becomes a fully recursive computation method as a bonus. To characterize the fire threat exposure from the Class B firebrand (ASTM E 108), we tested it in the cone calorimeter to obtain heat fluxes under the sample and temperatures at various sample locations. Heat fluxes as functions of time are used as inputs to the ignition and fire growth model to demonstrate changing boundary conditions for some fire-resistive materials, such as redwood, FRT plywood, and one-layer stucco-coated oriented strandboard (OSB). The effect of non-linearity of flame heights from the 100-kW ignition burner will also be presented at this conference in our re-evaluation of the ISO 9705 room test data (Dietenberger and Grexa, 1996).

CLASS B FIREBRAND TESTS IN THE CONE CALORIMETER

To understand the challenges presented in a typical fire scenario in the WUI, we burned the Class B firebrand of ASTM E 108 in the cone calorimeter (ASTM E 1354). A modified sample holder was used that allowed air flow into the sample and partially exposed the sample to air. This necessitated turning the cone heater to the vertical position to keep it out of the way, and we opted not to use the cone irradiance (although we may do so in the future). The ASTM E 108 test would have required a Bunsen burner for ignition to ensure a self-burning brand; instead, for our test, the brand was partially soaked in methanol bath. With ignition at the corners of the brand, the ensuing flame took several minutes to spread around the brand. The HRR history (Fig. 1) increases somewhat linearly to a broad peak value of 10 kW and then decreases gradually. Although a simple charring wood surface has a strong initial peak HRR and then decays approximately exponentially for many seconds, the phenomenon of flame spreading around the sample is rapid enough to result in a net increasing HRR with time. Once flame spreading is finished, the HRR should decay somewhat exponentially, but the increasing glowing HRR slows the decrease in the overall HRR. The fire growth process and the effect on the HRR profile is similarly imagined for flaming vegetations, roof fires, deck fires, and so on.

Heat flux from a burning firebrand, however, varies accordmg to size, distance, shape, viewfactor, and time-dependent HRR profile. For example, in our cone calorimeter test of a Class B brand, we were able to place one fluxmeter directly underneath the 150- by 150- by 60-mm wood crib with a 5-mm gap and 25 mm inward from the edge and another fluxmeter 45 mm outward from the wood crib. Heat flux data (Fig. 2) clearly show the effects of viewfactors of the developing flame on the measured value; the outside fluxmeter seems to mimic the HRR trend and has a peak heat flux of 6.7 kW/m^2, which is not enough to ignite most materials but can still char some materials. On the other hand, the underneath fluxmeter at first could not view the flame; when the flame came into view, the flux levels eventually reached 50 kW/m^2. After the flame subsided and the wood crib was glowing throughout, the flux became as high as 80 kW/m^2. This is the high flux that rapidly ignites most materials, including some fire-resistant materials, albeit with a little more time to ignition. This fact would make exterior cladding surfaces, such as roofs and decks, and unprotected interior flooring highly susceptible to ignition by the “worst case” firebrand. Therefore, designing fire-resistant claddings to prevent flame spreading or to avoid fire penetrating through the exposed layer after the inevitable ignition would be very desirable. One could observe similar ignition behavior for different species of wood materials, but their flame spreading behavior may be very different.

IGNITION SIMULATION WITH CHANGING CONDITIONS

Prediction of ignition that took into account changing boundary conditions, yet avoided the use of time-consuming finite difference methods, required an innovative mathematical formulation of the transient heat transfer problem. Dietenberger (2006) described a recursive analytical solution for transient heat and moisture transfer in a finitely thick hygroscopic material with step changes of certain boundary conditions. The solution for temperature change, $T(\hat{x},t)$, and moisture change, $U(\hat{x},t)$, profile due to boundary conditions of stepping changes in surface heat and moisture fluxes, $\dot{q}''(\ell,t)$ and $\dot{m}''(\ell,t)$, of such a material is presented here as

$$(1-\delta\delta^*)(a-b)\begin{Bmatrix} T(\hat{x},t) \\ U(\hat{x},t) \end{Bmatrix} \cong$$

$$\begin{aligned} &\sum_{i=0}^{n}\begin{Bmatrix} a-1/\alpha_m \\ -a\delta \end{Bmatrix}\left[\frac{\Delta\dot{q}''(\ell,t_i)}{K_{q,\ell}+\varepsilon\lambda K_{m,\ell}\delta}S(a,\hat{x},t-t_i)-\frac{\Delta\dot{q}''(0,t_i)}{K_{q,0}+\varepsilon\lambda K_{m,0}\delta}S(a,\ell-\hat{x},t-t_i)\right] \\ &+\sum_{i=0}^{n}\begin{Bmatrix} 1/\alpha_m-b \\ b\delta \end{Bmatrix}\left[\frac{\Delta\dot{q}''(\ell,t_i)}{K_{q,\ell}+\varepsilon\lambda K_{m,\ell}\delta}S(b,\hat{x},t-t_i)-\frac{\Delta\dot{q}''(0,t_i)}{K_{q,0}+\varepsilon\lambda K_{m,0}\delta}S(b,\ell-\hat{x},t-t_i)\right] \\ &+\sum_{i=0}^{n}\begin{Bmatrix} -a\delta^* \\ a-1/\alpha^* \end{Bmatrix}\left[\frac{\Delta\dot{m}''(\ell,t_i)}{K_{m,\ell}}S(a,\hat{x},t-t_i)-\frac{\Delta\dot{m}''(0,t_i)}{K_{m,0}}S(a,\ell-\hat{x},t-t_i)\right] \\ &+\sum_{i=0}^{n}\begin{Bmatrix} b\delta^* \\ 1/\alpha^*-b \end{Bmatrix}\left[\frac{\Delta\dot{m}''(\ell,t_i)}{K_{m,\ell}}S(b,\hat{x},t-t_i)-\frac{\Delta\dot{m}''(0,t_i)}{K_{m,0}}S(b,\ell-\hat{x},t-t_i)\right] \end{aligned} \quad (1)$$

with effective thermal diffusivity $\alpha^* = \dfrac{K_q+\varepsilon\lambda K_m\delta}{\rho C_q} = \alpha_q + \dfrac{\varepsilon\lambda K_m\delta}{\rho C_q}$ (2)

effective moist-thermo-gradient $\delta^* = \dfrac{\varepsilon\lambda K_m}{K_q+\varepsilon\lambda K_m\delta}$ (3)

mass diffusivity $\alpha_m = \dfrac{K_m}{\rho C_m}$ (4)

and coupling coefficients $\begin{Bmatrix} a \\ b \end{Bmatrix} = \left[\dfrac{\alpha_m+\alpha^*}{2\alpha_m\alpha_q}\right]\begin{Bmatrix} + \\ - \end{Bmatrix}\left[\sqrt{\left(\dfrac{\alpha_m+\alpha^*}{2\alpha_m\alpha_q}\right)^2-\dfrac{1}{\alpha_m\alpha_q}}\right]$ (5)

where $\hat{x}$ is dimensional depth, t is current time, K_q and K_m are thermal and moisture conductivity coefficients, C_q and C_m are heat and moisture capacities, ρ is dry body density, ε is ratio of vapor diffusion coefficient to coefficient of total moisture diffusion, λ is heat of phase change, δ is the thermo-moist-gradient coefficient, and $S(a,\hat{x},t)$ is the series expansion solution,

$$S(a,\hat{x},t) = \frac{t}{a\ell} + \ell\left\{\frac{3\hat{x}^2-\ell^2}{6\ell^2} - \frac{2}{\pi^2}\sum_{n=1}^{\infty}\frac{(-1)^n}{n^2}\exp\left[\frac{-t}{a}\left(\frac{n\pi}{\ell}\right)^2\right]\cos\left(\frac{n\pi\hat{x}}{\ell}\right)\right\} \quad (6)$$

In Equation (6), the term b replaces the term a when appropriate for Equation (1). When the material is oven dried, there is no moisture ($\varepsilon = 0$) for transferring latent heat λ in the vapor phase, making Equation (3) equal to zero, which then reduces Equation (1) to the classical heat conduction solution. Dietenberger (2006) demonstrated the impact of redwood with about 14% moisture content, in which the transient latent heat contribution adds 32% to the steady value of thermal conductivity (see Eq. (2)). Redwood then dries quickly when temperatures go above 100°C, which has the effect of reducing thermal conductivity K_q significantly below its nominal value at 14%moisture content. Thermal conductivity will increase again perhaps nonlinearly as temperature rises further, mostly due to internal radiant heat exchanges. If irradiance $\dot{q}''_r$ is applied to one surface, the material responds with radiative and convective cooling on the exposed side and conductive cooling on the unexposed side, as in the boundary conditions,

$$\left.\begin{aligned}\Delta\dot{q}''(\ell,t_i) &= \alpha_{s,i}\dot{q}''_r(t_i)+\varepsilon_{s,i}\sigma[T_a{}^4(t_i)-T^4(\ell,t_i)]+h_{c,i}[T_a(t_i)-T(\ell,t_i)]\\ &\quad -H(t_i-t_1)\left\{\alpha_{s,i}\dot{q}''_r(t_{i-1})+\varepsilon_{s,i}\sigma[T_a{}^4(t_{i-1})-T^4(\ell,t_{i-1})]+h_{c,i}[T_a(t_{i-1})-T(\ell,t_{i-1})]\right\}\\ \Delta\dot{q}''(0,t_i) &= C_{\text{insulate}}[T(0,t_i)-T_a(t_i)]-H(t_i-t_1)C_{\text{insulate}}[T(0,t_{i-1})-T_a(t_{i-1})]\end{aligned}\right\} \quad (7)$$

then eventually the predicted surface temperatures will reach a steady-state value in which convective and radiative heat losses to the air and conductive heat losses to backside insulation equal radiant energy absorbed. The heaviside function $H(t_i - t_1)$ is used to specify that prior to heat exposure the sample is at a uniform temperature and therefore has zero heat fluxes at both surfaces. The summation in Equation (1) is quite unwieldy until it is realized the expansion solution in Equation (6) has exponential terms to convert it into a fully recursive solution. It was also found that expansion to the eighth term permitted three-significant-digit accuracy, making the solution method easily implemented in the Excel (Microsoft Corp., Redmond, Washington) spreadsheet and also highly accurate even for thermally thick materials. It also made the method highly competitive with the finite difference methods in that it uses less memory and is valid for a wide range of Fourier and Biot numbers. If the irradiance is high enough, then the surface will reach ignition temperature T_{ig} prior to reaching steady-state temperature. To more accurately capture the time at ignition, we used time steps of 1 s or less.

As can be seen from Equation (7), changes in the boundary conditions with time can be used. That is, we can arbitrarily vary irradiances, convective flow, atmospheric temperature, and surface conditions with time. If the sample has moisture content, then Equation (7) should include a latent heat component, and additional moisture flow rate equations for each surface should be used along with Equation (7). In principle, we can use this method to forecast moisture conditions of the combustible item (which will be discussed in a future publication). The method can also be extended to multi-layered samples in which interfacial zones can be treated as "conductive backside cooling" heat transfers. To consider ignition due to flame impingement, we have the imposed heat flux from the 100-kW propane ignition burner (or the firebrand flames), $\dot{q}''_w$, in our room burn tests to use in place of the term, $\alpha_s \dot{q}''_r + \varepsilon_s \sigma (T_a^4 - T(\ell,t)^4) + h_{ci}(T_a - T(\ell,t))$ in Equation (7) as

$$\dot{q}''_w = \sigma(\alpha_s \varepsilon_f T_f^4 + \varepsilon_s (1-\varepsilon_f) T_a^4 - \varepsilon_s T(\ell,t)^4) + h_{cf}(T_f - T(\ell,t)) \quad (8)$$

The parameters that are known in the case of fluxmeters in the wall are $\dot{q}''_w = 55\,\mathrm{kW/m^2}$, $T(\ell,t) = 298\,\mathrm{K}$ and surface absorptivity and emissivity as $a_s = \varepsilon_s = 0.97$. Using averaged measured flame temperature, $T_f = 1173\,\mathrm{K}$, we derived values of flame emissivity and convective coefficient as $e_f = 0.391$ and $h_{cf} = 0.0165\mathrm{kWm^2\,K}$ to reproduce the fluxmeter heat flux. Our test materials typically have lower surface emissivity, $\varepsilon_s = 0.88$, and using the above values for other parameters, the imposed heat flux becomes 51 kW/m^2 instead. Therefore we would expect the time to ignition on the wall to correlate best with the cone heater flux of 50 kW/m^2, as found by Karlson (1993). However, he used a multiplication factor of 1.7 times the time to ignition from the cone calorimeter to obtain the actual time to ignition for the room test. We note that using a manual valve to ensure a 100-kW level could mean a time response of 5 or 11 s to the 90 % level, which in turn provides the requisite significant effect on time to ignition (Dietenberger and Grexa, 1996) equivalent to Karlson's multiplication factor. In the case of the tested firebrand for the imposition of heat fluxes on the samples, the results in Figure 2 show that even various terms in Equation (8) need to be re-evaluated for each time step as the flame emissivity and convective heat transfer coefficient change as the fire engulfs the firebrand. In early fire growth, we note the flame is non-impinging and not viewed by the underneath fluxmeter, meaning that Equation (8) is not applied during this material heating phase.

FIRE GROWTH SIMULATION WITH CHANGING CONDITIONS

Dietenberger and Grexa (1996), reporting on IS09705 tests, described the complex-variable Laplace transform solution of the Duhamel integral for flame spread, HRR, and pyrolysis area that involved four stages requiring solution restarts: (1) ignited corner area due to a sluggish propane burner, (2) upward spread of corner flame to the ceiling, (3) lateral spread of top-wall flame for the unlined ceiling, and (4) the pre-flashover rapid downward spreading of flame on the entire three walls. This analytical solution was modified for application to the changing conditions of the WUI fire scenario and is reported here. After the initial phase of ignition, the later phases of fire growth are similar in that they involve the flame spreading process and, depending on the occasion, the forcible ignited areas, such as swift increase of pilot burner output from 100 to 300 kW at 10 min in the ISO9705 test. First step in the analysis is the description of the extended flame flux profile as an imposed flux applied over surface distance y_c followed by an exponential decay with characteristic length δ_f, as in

$$\dot{q}''_{wf}(y) = \dot{q}''_{w0}\left[H(y) + \left(\exp\left\{\frac{-(y-y_c)}{\delta_f}\right\} - 1\right)H(y-y_c)\right] \qquad (9)$$

where *H(y)* is the heaviside function. In the case where the flame is only from the material burning (by imagining the ignition burner to provide only external radiant flux by being away from the wall), Kulkarni et al. (1994) reported the following experimental results. Heat fluxes are 24.3 kW/m^2 for Douglas-fir particle board and 34.5 kW/ m^2 for cardboard. With the length of constant flux,y_c, identified with the pyrolysis front, y_p , the characteristic length was found to be proportional to extended flame length and correlated as, $\delta_f = (y_f - y_p)/c_f$, with $c_f = 1.37$. However, with the pilot burner flames merging with the material flames in the IS09705 test protocol, the more appropriate data to use are reported by Kokkala and Heinila (1991). Using their figures of the flame flux profiles for different burner sizes and outputs, we estimated the values for the ratio of extended flame length over characteristic length to vary from 1.2 to 1.4, for which we found 1.3 to be optimum. With this spatial profile of flame heat flux, we then analyzed for the quasi-steady speed, v_p , of the pyrolysis front by using the formula $y - y_g = v_p(t_{ig} - t)$ in Equation (9) to represent the sliding movement of imposed heat flux profile over a given spot until ignition temperature is reached. With this substitution, the Duhamel's supposition integral is the convolution of the material's thermal response to a constant imposed flux with the time changing imposed flux as in

$$T_{ig} - T_m = \frac{d(T(\ell,t))}{dt} \otimes \dot{q}''_{wf}(v_p(t_{ig} - t) + y_{ig}) = (T(l,t)) \otimes \frac{d\dot{q}''_{wf}(y_{ig} - v_p(t - t_{ig}))}{dt} \qquad (10)$$

where the integration is taken from zero to the time of ignition, t_{ig}, to correspond to ignition temperature, T_{ig}. We note that Equation (10) becomes exactly Equation (1) (with moisture terms zeroed in Eq. (3), at the surface $x = l$, and T_m is the preheated surface temperature in response to other heat sources), provided the heat flux profile of Equation (9) is approximated by incremental flux changes at every time step, up to the time of ignition. Because it is possible to have a wide variation in the characteristic flame length, depending on the direction of the flame spread, then the time step sizes will have to be highly adaptable to ensure a reasonably accurate and efficient descretization of Equation (9) for its use in Equation (1). If there are multiple flame spread directions on multiple combustible items, then it would be impossible to determine the optimum time steps. This is the fundamental reason why the CFD codes, such as the FDS, will fail to predict some types of flame spread problems. To get around this problem, the intricate analytical solution to Equation (10) (instead of a descretization solution) for both thermally thick and thermally thin materials and with interpolation between the regimes is given (Dietenberger, 1991) as

$$\delta_f = v_F \tau_m = v_F K_q \rho C_p \left(\frac{T_{ig} - T_m}{\dot{q}''_{w0} - \dot{q}''_{ig}} \right)^2 \left(\frac{1}{2} + \sqrt{\frac{1}{4} + \left(\frac{K_q (T_{ig} - T_m)}{\ell (\dot{q}''_{w0} - \dot{q}''_{ig})} \right)^{1.3}} \right)^{\left(\frac{-2}{1.3}\right)} \qquad (11)$$

where $\dot{q}''_{ig} = \varepsilon_s \sigma (T_{ig}^4 - T(\ell,0)^4) + h_c (T_{ig} - T(\ell,0))$ (12)

One then realizes that all the material's parameters for thermal response are contained in the material time constant, τ_m, during flame spreading. Closer examination of Equation (11) shows that the flame spread rate, v_F , can be made quite small with large values for thermal conductivity, material density, heat capacity, material ignition temperature, and material thickness or with small values for preheated surface temperature, flame heat flux, and flame footprint. Obviously, to completely stop flame spreading for any direction, the flame flux at initial time (via Eq. (8)) needs to be reduced to the critical heat flux needed for ignition (via Eq. (12)). Therefore, as the flame spreads away from a radiant source, the pyrolysis rates under the leading flame will likely diminish, leading to smaller flame sizes and smaller values for the flame emissivity in Equation (8). The flame temperature will likely decrease, too, due to cooler input air flow as well as a decreasing heat of combustion for diluted wood volatiles associated with the lowered imposed fluxes. The surface temperature at piloted ignition can also increase as well due to wood volatile depleting after long-time exposure to low heat fluxes. This process continues until the cooling flux at ignition temperature becomes equal to imposed flame flux for stopping flame spread. The flame itself may continue to exist until the char layer has become deep enough to effectively deplete the wood volatiles under the regions of high radiant source. The use of fire retardants merely improves upon this flame spread halting, even to the point of diminishing upward flame spreading under a strong radiant source. The main point made in this overall discussion is that the supposed "constant" fire properties used in Equation (11) are also changing with time, especially for wood and treated materials.

As the next step in analytical modeling of fire growth, the flame oversize area, A_f - A_p , as a non-linear function of HRR, Q_t, and flame width, w, for the corner flame (Dietenberger and Grexa, 1996) is linearized at each time step as

$$2w(y_f - y_p) = 0.0433(2w)^{1/3} Q_t^{2/3} \approx A_{fm} + \frac{\partial A_f}{\partial Q_t}(Q_t - Q_m) + \frac{\partial A_f}{\partial A_p}(A_p - A_{pm}) = c_f (a + bA_p + cQ_t) \qquad (13)$$

The flame area for other geometries, such as the single vertical wall, a tunnel ceiling, or a circular pool fire, can be similarly linearized for their respective nonlinear functions. The fire growth problem, as a rearrangement to Equation (11), can now be stated concisely as the Voltera type integral as

$$\frac{dA_p}{dt} = 2wv_F = \frac{a + bA_p + cQ_t}{\tau_m} + A_{ig,i}\Lambda(t - t_i) \qquad (14)$$

where the total HRR is given by a sum of ignition-burner and material-flame-spreading heat release rates as

$$Q_t = \sum_i \Delta Q_{b,i} H(t-t_i) + \sum_i A_p(t_i) Q''_m(t-t_i) + \int_0^{t-t_i} Q''_m(t-t_i-\xi)\dot{A}_p \, d\xi \quad (15)$$

and

$$Q''_m(t) = Q''_{m,\mathrm{ig}} H(t)\exp(-\omega_m t) \qquad (16)$$

whereas an exponentially decaying HRR profile (with decay coefficient, ω_m) is assumed for a given sample surface, with the peak HRR flux, $Q''_{m,\mathrm{ig}}$,also changing with time as a result of the changing radiant source. The index i provides tracking of changes to the coefficients in Equation (14) with time steps or to "instantaneous" ignition of newly covered areas for step increases of the burner. The recursive Laplace solution to Equation (14) (with Eqs. (13), (15), and (16) substituted into it and various terms treated as constant during the time step) is given for each time step as (with $t^* = t - t_i > 0$)

$$A_p(t) = \left(\frac{a + c(Q_{mi} - A_{pi}Q''_{m,\mathrm{ig}} + Q_{bi} + \Delta Q_{bi})}{\tau_m} + A_{pi}\omega_m\right)\left(\frac{\exp(s_1 t^*) - \exp(s_2 t^*)}{s_1 - s_2}\right)$$
$$+ A_{pi}\left(\frac{s_1\exp(s_1 t^*) - s_2\exp(s_2 t^*)}{s_1 - s_2}\right) + \left(\frac{a + c(Q_{bi} + \Delta Q_{bi})}{\tau_m}\right)\left(\frac{\omega_m}{s_1 - s_2}\right)\left(\frac{\exp(s_1 t^*) - 1}{s_1} - \frac{\exp(s_2 t^*) - 1}{s_2}\right) \quad (17)$$

$$Q_t(t) = Q_b(t) + Q_m(t) = Q_{bi} + \Delta Q_{bi} + \left(\frac{(a + cQ_{bi})Q''_{m,\mathrm{ig}} - b(Q_{mi} - A_{\mathrm{p}i}Q''_{m,\mathrm{ig}})}{\tau_m}\right)\left(\frac{\exp(s_1 t^*) - \exp(s_2 t^*)}{s_1 - s_2}\right)$$
$$+ \frac{cQ''_{m,\mathrm{ig}}}{\tau_\mathrm{m}}\Delta Q_{bi}\left(\frac{\exp(s_1 t^*) - \exp(s_2 t^*)}{s_1 - s_2}\right) + Q_{mi}\left(\frac{s_1\exp(s_1 t^*) - s_2\exp(s_2 t^*)}{s_1 - s_2}\right) \quad (18)$$

where growth acceleration coefficients (in complex variable form) are

$$s_i = \frac{b + cQ''_{m,\mathrm{ig}} - \omega_m\tau_m}{2\tau_m} - (-1)^i\sqrt{\left(\frac{b + cQ''_{m,\mathrm{ig}} - \omega_m\tau_m}{2\tau_m}\right)^2 + \frac{b\omega_m}{\tau_m}} \qquad (19)$$

For brevity, we define the recursive terms, $A_{pi} = A_{\mathrm{ig},i} + A_p(t_i)$, $Q_{bi} = Q_b(t_i)$, and $Q_{mi} = Q''_{m,\mathrm{ig}} A_{\mathrm{ig},i} + Q_m(t_i)$. The size of the overflame area as a function of time is merely given with Equation (13). Because Equations (17) and (18) are framed in a recursive form, the coefficients and parameters treated as constants during a time step can be allowed to vary from time step to time step. Indeed, the material time constant, τ_m, is actually a fairly strong function of time via the changing preheat temperature, T_m , in Equation (11), which in turn is calculated with Equation (1) using the time-changing external radiant flux boundary conditions. Therefore, one could conceive that the overall fire growth can switch from a damped fire spread to an accelerative fire spread, or vice versa, through the mere time variation of the material time constant. Because the roots are considered complex numbers, the above solutions are considered to be in the complex variable domain. Specialized computer algorithms were developed for complex evaluations so that the above functions could be programmed directly as FORTRAN code called by the Excel spreadsheet. We note that specialized numerical deconvolutions and certain corrections were also applied to the oxygen and water vapor signals to synchronize them with the rapid responding CO/CO_2 and laser smoke data of the cone calorimeter. The reprocessed cone data were then used to recalculate the more exacting heat release rate of the Class B firebrand (see Fig. 1) for direct comparison with predictions from fire growth Equation (18). Because the firebrand is made of Douglas-fir, we extended the derived fire properties of ignition and heat release flux profile from our previous tests of Douglas-fir wood products from our IS09705 room test series (Dietenberger and Grexa, 1996). With the least-squares solver of the Excel spreadsheet, we are determining the values of the coefficients in Equations (8) and (13) that provided the best fit to the data. An application of exterior heat flux to the firebrand would certainly enhance the heat release rate, which we could do by using the cone heater in its vertical position. Because of the recursive nature of fire growth Equations (17) and (18), it should be possible to consider various changing conditions without the need for recalibrating the coefficients.

CONCLUSION

Introductory discussions on wildfire threats to structures and their mitigation has shown the need to understand damage, ignition, and fire growth as exposed to changing conditions on realistic combustible items, including those considered to be fire resistive. We also believe that by providing a fire hazard tool based on fire growth algorithms associated with ornamental vegetations and fire-resistive exteriors in changing environments as proposed here, the client will be able to find an optimum and economical approach for fire-safe construction and landscaping. More specifically, the calculations should ultimately be able to provide (1) the fuel clearance (both vegetation and structure) needed for mitigating large fire threats of high radiant flux/flame impingements on structures and (2) the mitigation of firebrand threat (from both woodland and neighborhood) to an uninvolved structure with several different and economical fire resistive claddings.

REFERENCES

Dietenberger, Mark A. 1991. Piloted ignition and flame spread on composite solid fuels in extreme environments. Ph.D. Dissertation, University of Dayton.

Dietenberger, MA. 2006. Using a quasi-heat-pulse method to determine heat and moisture transfer properties for porous orthotropic wood products. J. Thermal Analysis and Calorimetry 83(1):97-106.

Dietenberger, MA., and Grexa, O. 1996. Analytical model of flame spread in full-scale room/corner tests (ISO9705), 6th Int. Fire & Materials Conf., San Antonio, TX, Feb. 22-23, Interscience Comm. Ltd., pp. 211-222.

Dietenberger, Mark A., White, Robert H. 2001. Reaction-to-fire testing and modeling for wood products. In: Twelfth Annual BCC Conference on Flame Retardancy, May 21-23, 2001, Stamford, CT. Business

Communications Co., Inc., Norwalk, CT. pp. 54-69. [http://www.fpl.fs.fed.us/documnts/pdf2001/diete01b.pdf]

Karlsson, Bjorn. 1993. A mathematical model for calculating heat release rate in the room corner test. Fire Safety Jorunal 20:93-113.

Kokkala, Matti, and Heinila, Markol. 1991. Flame height, temperature, and heat flux measurements on a flame in an open corner of walls. Project 5 of the EUROFIC fire research programme.

Kulkarni, A.K., Brehob, E., Manohar, S., and Nair R. 1994. Turbulent upward flame spread on a vertical wall under external radiation. NIST-GCR-94-638.

Manzello, S.L., Cleary, T.G., Shields, J.R., and Yang, J.C. 2006, On the ignition of fuel beds by firebrands. Fire and Materials 30:7-87.

FIGURE 1

HEAT RELEASE RATE OF CLASS B BRAND

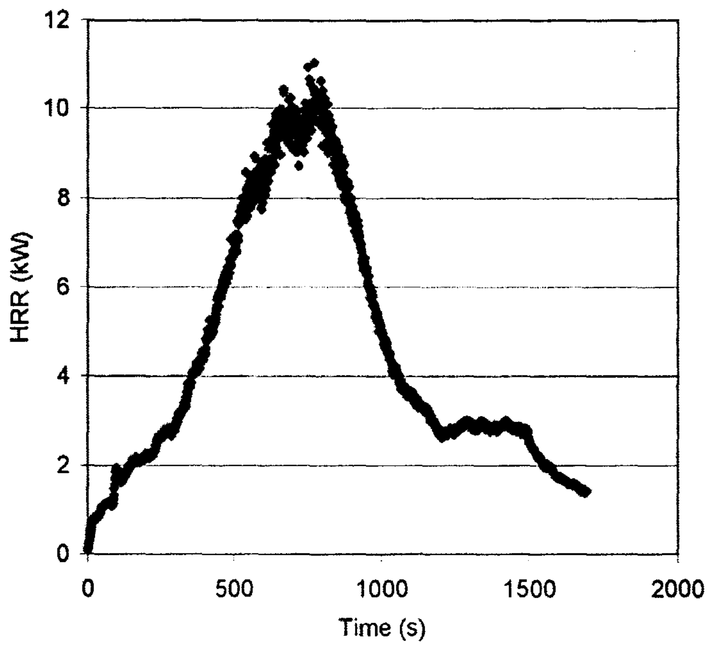

FIGURE 2

CLASS B BRAND HEAT FLUXES

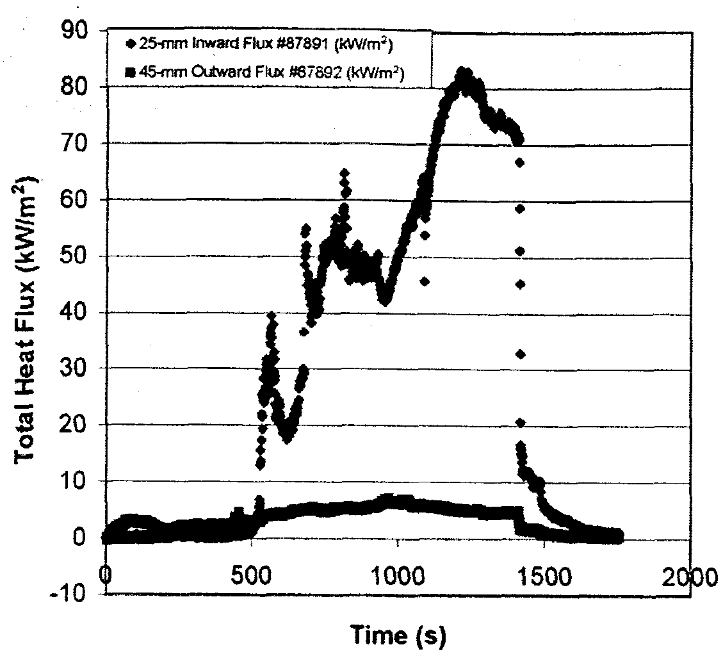

PROCEEDINGS OF THE CONFERENCE ON RECENT ADVANCES IN FLAME RETARDANCY OF POLYMERIC MATERIALS

VOLUME XVII

APPLICATIONS, RESEARCH AND INDUSTRIAL DEVELOPMENT, MARKETS

CHM007G

BCC Research
70 New Canaan Ave
Norwalk, CT 06850
Phone: 866-285-7215 (sales)
Web Address: www.bccresearch.com
E-mail: sales@bccresearch.com
ISBN:1-59623-221-8